Effect of a shear flow on the planform of thermal convection in a fluid of variable viscosity

Philip Hall
Mathematics Department, Manchester University, Manchester M3 9PL, United Kingdom

Robert E. Kelly
Mechanical, Aerospace and Nuclear Engineering Department, University of California, Los Angeles, California 90024-1597
(Received 1 September 1993; revised manuscript received 13 March 1995)

It is well known that if the variation with temperature of viscosity is taken into account, the onset of convection in an infinite layer of fluid that is heated from below takes the form of hexagonal convection cells. It is also well known that in a sufficiently strong shear flow, rolls aligned with the flow direction are the preferred mode of convection. Here the process by which a steady or unsteady shear flow destroys the usual hexagonal cell pattern is investigated. The critical size of the shear flow that enables rolls to be established at the onset of convection is determined for the case when the stress is prescribed at the boundaries.

PACS number(s): 47.20.−k

I. INTRODUCTION

Our concern is with the manner in which steady and unsteady shear flows remove the preference for a heated fluid layer to become convectively unstable with regard to hexagonal cells. It is well known that if variation with temperature of viscosity is taken into account, the onset of convection without shear is in the form of hexagonal cells, with the direction of flow at the center of the cell dependent on the sign of the change in viscosity due to temperature; see Segel and Stuart [1], Palm, Ellingsen, and Gjevik [2], Segel [3], and Busse [4]. Convection occurs via a subcritical bifurcation to the hexagonal cell pattern rather than via supercritical bifurcation to convection rolls as occurs with a Boussinesq fluid. After convection has been established, a further increase in the Rayleigh number for the flow causes the hexagonal pattern to become unstable and a roll mode is established. If the Rayleigh number is subsequently decreased, the roll pattern persists to a value of the Rayleigh number lower than the one at which rolls first appear. This hysteresis is again a direct consequence of the subcritical nature of the bifurcation to hexagonal cells. Another consequence of this subcritical bifurcation is that the onset of convection occurs discontinuously when the Rayleigh number is increased.

Suppose next that the heated fluid layer is subjected to a shear flow caused by either a pressure gradient or the motion of the channel walls; a recent review of this topic has been given by Kelly [5]. It can be shown that if the shear flow is in, say, the x direction, then rolls aligned with the x axis (i.e., longitudinal rolls) are not affected by the flow and the critical Rayleigh number for the onset of such rolls is unchanged from its value for the zero flow case. However, if the horizontal aspect ratios are large, all other rolls are stabilized by the shear flow on a linear basis and for small flow rates the critical Rayleigh number is increased by an amount proportional to the square of the flow Reynolds number. The preference for longitudinal rolls in fully developed, large aspect ratio channel flow has been seen in many experiments, although hexagonal convection has sometimes been observed at very small flow rates (Ostrach and Kamotani [6]). Expressions for the critical Rayleigh number for a Boussinesq fluid at low Reynolds numbers for the onset of rolls of arbitrary orientation have been given for Couette flow by Ingersoll [7], whereas Müller, Lücke, and Kamps [8] have given results for Poiseuille flow.

Thus, in the presence of a shear flow, any roll disturbance not aligned with the shear flow has a critical Rayleigh number which, for small Reynolds numbers, increases monotonically with the Reynolds number. Since a hexagonal convection cell is formed by the combination of three roll cells with axes parallel to the sides of an equilateral triangle, it can be expected that at some stage the preference for the onset of convection in a non-Boussinesq fluid to take the form of hexagonal cells will be destroyed. We concern ourselves in this paper with details of how a shear flow gradually decreases the preference for hexagonal cells. This process has been described qualitatively for a fluid with a prescribed variable mean temperature gradient by Yoshizaki [9], but he did not predict numerical values of the critical shear, nor did he examine in detail all the bifurcations possible for this problem.

The procedure adopted in the rest of the paper is as follows. In Sec. II we shall derive a system of amplitude equations that are the appropriate generalizations of the equations from [3] in the presence of a weak shear flow. In fact, we will allow the shear flow to be nonplanar and unsteady, but we shall consider only slowly varying time periodic small amplitude flows. In Sec. III we shall investigate the bifurcation structure of these equations. This will enable us to describe the process by which hexagonal cells are destroyed by a shear flow. In Sec. IV we shall draw some conclusions.

II. THE AMPLITUDE EQUATIONS FOR CONVECTION IN A WEAK, SLOWLY OSCILLATING SHEAR FLOW

To begin with, we determine the effect of a weak shear flow on the linear Bénard convection problem for a Boussinesq fluid. Suppose then that such a fluid occupies the region $0<z<d$, and that the wall $z=0$ is maintained at a temperature $T_0+\Delta T$, whereas the upper one has temperature T_0. We suppose further that the lower wall has velocities $(\kappa/d)\lambda_1\cos\omega\tau$, $(\kappa/d)\lambda_2\cos[\omega\tau+\gamma]$ in the x and y directions. Here κ is the thermal diffusivity, and τ is a dimensionless time variable based on $d^2\kappa^{-1}$. The dimensionless parameter ω relates the time scale of the flow oscillations to the diffusive time scale. Here we shall concern ourselves with the low frequency case $\omega\ll 1$, but a more general discussion of the linear case can be found in Kelly and Hu [10,11]. We shall make the further assumption that the amplitude of the flow oscillations is small and therefore we take λ_1 and λ_2 to be small; more precisely, we identify the limit $\omega\to 0$ with $\lambda_1,\lambda_2\sim O(\omega^{1/2})$ as being the crucial case for small amplitudes and frequencies. This choice, made using the ideas of DiPrima and Stuart [12], ensures that the Floquet exponent associated with the stability problem has comparable real and imaginary parts. We therefore write

$$\lambda_1=\hat{\lambda}_1\delta,\quad \lambda_2=\hat{\lambda}_2\delta,\quad \omega=\Omega\delta^2$$

and consider the limit $\delta\to 0$ with $\hat{\lambda}_1,\hat{\lambda}_2$ and Ω held fixed.

If we use κ/d as a velocity scale, then for small values of δ the basic flow may be written in the form

$$\mathbf{u}=\delta\{(\hat{\lambda}_1\cos[\Omega t],\hat{\lambda}_2\cos[\Omega t+\gamma],0)\}(1-z)+O(\delta^3)\ , \tag{2.1}$$

where $t=\delta^2\tau$ and z has been scaled on d. The basic temperature field is, of course, not dependent on this velocity field and is given by

$$T=T_0+\Delta T z\ . \tag{2.2}$$

We now perturb the above basic state to a disturbance periodic in the x,y directions with wavelengths $2\pi/k_x, 2\pi/k_y$. Thus we write, for example, the perturbed normal velocity component w in the form

$$w=\{w_0(t,z)+\delta w_1(t,z)+\delta^2 w_2(t,z)+\cdots\}\times\exp i\left\{k_x\left[x-\frac{\hat{\lambda}_1\sin\Omega t}{\delta 2\Omega}\right]+k_y\left[y-\frac{\hat{\lambda}_2\sin[\Omega t+\gamma]}{\delta 2\Omega}\right]\right\}\ . \tag{2.3}$$

Here we have introduced extra time-dependent terms inside the exponential factor in order to satisfy in a more convenient form the $O(\delta)$ solvability condition obtained in the linear stability problem. (That problem yields a time-dependent wave velocity and we are in effect choosing to work in a coordinate system moving with the fluid midway between the two walls.) After the usual manipulations, we find that the linear stability equations can be expressed in the form

$$[\sigma^{-1}L-\partial_z^2+k_c^2][\partial_z^2-k_c^2][w_0+\delta w_1+\cdots]=-k_c^2\mathrm{Ra}[\theta_0+\delta\theta_1+\cdots]\ ,$$

$$[L-\partial_z^2+k_c^2][\theta_0+\delta\theta_1+\cdots]=[w_0+\delta w_1+\cdots]\ ,$$

where Ra is the Rayleigh number, σ is the Prandtl number, $k_c^2=k_x^2+k_y^2$, and the operator

$$L\equiv\left\{\delta^2\partial_t+(ik_x\delta\hat{\lambda}_1\cos\Omega t+ik_y\delta\hat{\lambda}_2\cos[\Omega t+\gamma])\times[1-z]-\frac{ik_x}{2}\delta\hat{\lambda}_1\cos\Omega t-\frac{ik_y}{2}\delta\hat{\lambda}_2\cos[\Omega t+\gamma]\right\}\ .$$

The Rayleigh number is expanded as

$$\mathrm{Ra}=R_{0,c}+\delta^2R_2+\cdots\ . \tag{2.4}$$

The leading order problem for (w_0,θ_0) is

$$(\partial_z^2-k_c^2)^2w_0=k_c^2R_0\theta_0\ ,$$

$$(\partial_z^2-k_c^2)\theta_0=-w_0\ .$$

For convenience, we will assume that the perturbed velocity field must satisfy fixed stress surface conditions at $z=0,1$. While this assumption tends to make our problem somewhat artificial, it enables us to make analytical progress most simply with the nonlinear problem to be discussed shortly and probably gives qualitatively correct results for the low frequency case discussed in this paper. Thus, if the velocity perturbation satisfies the zero stress conditions at $z=0,1$ and the boundaries are isothermal, we obtain the usual eigenrelation

$$(k_c^2+\pi^2)^3=k_c^2R_{0c}\ , \tag{2.5}$$

so $R_{0,c}=27\pi^4/4$ and $k_c=\pi/\sqrt{2}$. The corresponding eigensolution is

$$(\theta_0,w_0)=A(t)\sin\pi z(1,\pi^2+k_c^2)\ , \tag{2.6}$$

where A is an amplitude function to be determined at higher order. At order δ we find that the solvability condition required for a solution of that system to exist is automatically satisfied because of our insertion of the correct time-dependent factor in the exponential term of (2.3). We find that

$$(w_1,\theta_1)=i\mathcal{F}A(t)(\hat{w}_1,\hat{\theta}_1)\ ,$$

where $\mathcal{F}=\hat{\lambda}_1k_x\cos\Omega t+\hat{\lambda}_2k_y\cos[\Omega t+\gamma]$, and

$$(d_z^2-k_c^2)^2\hat{w}_1-k_c^2R_0\hat{\theta}_1=-\sigma^{-1}(\pi^2+k_c^2)^2(\tfrac{1}{2}-z)\sin\pi z\ ,$$

$$(d_z^2-k_c^2)\hat{\theta}_1+\hat{w}_1=(1/2-z)\sin\pi z\ , \tag{2.7}$$

$$\hat{w}_1=\hat{w}_1''=\hat{\theta}_1=0,\quad z=0,1\ .$$

At order δ^2 we find that the differential system for w_2 has a solution if

$$\Sigma\frac{dA}{dt}=\mu R_2A-\lambda^*\mathcal{F}^2A\ , \tag{2.8}$$

where

$$\Sigma=\frac{9\pi^4(1+(1/\sigma)}{4}\ , \tag{2.9}$$

$$\mu=\frac{\pi^2}{2}\ , \tag{2.10}$$

$$\lambda^*=\int_0^1 \sin\pi z\left\{\sigma^{-1}(z-\tfrac{1}{2})\left[(\hat{w}_1''-\hat{w}_1\pi^2/2)+\frac{9\pi^4}{4}\hat{\theta}_1\right]\right\}dz\ , \tag{2.11}$$

and $\lambda^*=\lambda^*(\sigma)$ is always positive.

The linear amplitude equation (2.8) can be integrated to give

$$A=a_0\exp\frac{\mu R_2 t-\lambda^*\int^t \mathcal{F}^2 dt}{\Sigma}\ ,$$

where a_0 is a constant. The neutral stability case is then defined by

$$\mu R_2\frac{2\pi}{\Omega}-\lambda^*\int_0^{2\pi/\Omega}\mathcal{F}^2 dt=0, \tag{2.12}$$

so that

$$\mu R_2=\frac{\lambda^*}{2}\{(\hat{\lambda}_1 k_x)^2+(\hat{\lambda}_2 k_y)^2+2k_x k_y\hat{\lambda}_1\hat{\lambda}_2\cos\gamma\}\ . \tag{2.13}$$

The wave numbers k_x and k_y must be constrained such that

$$k_x^2+k_y^2=\frac{\pi^2}{2}\ ,$$

so that writing $k_x=(\pi/\sqrt{2})\cos\theta$, $k_y=(\pi/\sqrt{2})\sin\theta$ enables us to express (2.13) in the form

$$\mu R_2=\frac{\lambda^*\pi^2}{4}\{\hat{\lambda}_1^2\cos^2\theta+\hat{\lambda}_2^2\sin^2\theta+2\hat{\lambda}_1\hat{\lambda}_2\cos\gamma\sin\theta\cos\theta\}\ . \tag{2.14}$$

The right-hand side above is always nonnegative so that the shear generally has a stabilizing effect on the flow. However, we can see for the cases $(\hat{\lambda}_1=0,\theta=0)$ and $(\hat{\lambda}_2=0,\theta=\pi/2)$ that $R_2=0$. Thus in these cases we recover the known result that, at this order, rolls aligned with the flow are not affected by the flow. Further discussion of (2.13) can be found in [10]. Here we wish to concentrate on the role of the shear flow on the pattern selection problem in the weakly nonlinear regime.

In fact, having found the linear form for the amplitude equation in a weak shear flow, we can simply use the results of previous authors to extend the analysis to the weakly nonlinear regime. We refer to [1,3] for the slightly non-Boussinesq fluid. The problem studied by the latter authors concerned the pattern selection problem involving rolls and hexagons. Using the notation of the present paper, it was shown by the above authors that the selection problem reduces to the investigation of the nonlinear interaction of modes with wave numbers $(k_x,k_y)=(\pi/\sqrt{2})(\frac{1}{2},-\sqrt{3}/2)$, $(k_x,k_y)=(\pi/\sqrt{2})(\frac{1}{2},\sqrt{3}/2)$, and $(k_x,k_y)=(\pi/\sqrt{2})(1,0)$. In the absence of a shear flow, the normal velocity component expands as

$$w=\delta\sin\pi z\{XE_1+YE_2+ZE_3\}+\text{c.c.}+\cdots\ ,$$

with

$$E_1=\exp\frac{i\pi}{\sqrt{2}}\left[\frac{x}{2}-\frac{\sqrt{3}}{2}y\right]\ ,$$

$$E_2=\exp\frac{i\pi}{\sqrt{2}}\left[\frac{x}{2}+\frac{\sqrt{3}}{2}y\right]\ ,$$

$$E_3=\exp\frac{i\pi}{\sqrt{2}}x\ .$$

If the variation of viscosity is assumed to be small, in fact $0(\delta)$, then it is found that the equations to determine the complex amplitudes X, Y, and Z are

$$\Sigma\dot{X}=\epsilon X-a\bar{Y}Z-X\{R_1|X|^2+P|Y|^2+P|Z|^2\}\ , \tag{2.15a}$$

$$\Sigma\dot{Y}=\epsilon Y-a\bar{X}Z-Y\{R_1|Y|^2+P|X|^2+P|Z|^2\}\ , \tag{2.15b}$$

$$\Sigma\dot{Z}=\epsilon Z-aXY-Z\{R_1|Z|^2+P|X|^2+P|Y|^2\}\ , \tag{2.15c}$$

where an overbar denotes the complex conjugate, $\epsilon=\mu R_2$, and a, R_1, and P are the constants defined in [3]. Because we have complex amplitudes, (2.15a)–(2.15c) correspond to those of Segal [3]. Note, however, that similar equations can be found if the variations with temperature of other fluid properties are taken into account; see, for example, [4]. In order to determine the effects of a weak, low frequency, unsteady, nonplanar shear flow upon pattern development, one can essentially combine the analyses leading to (2.8) and (2.15a)–(2.15c). In order to do so, it is first necessary to define new variables $\hat{x}$ and $\hat{y}$ by

$$\hat{x}=x-\frac{\hat{\lambda}_1\sin\Omega t}{2\Omega\delta},\quad \hat{y}=y-\frac{\hat{\lambda}_2\sin[\Omega t+\gamma]}{2\Omega\delta}\ ,$$

and then x and y appearing in the definitions of E_1 and E_2 are replaced by $\hat{x}$ and $\hat{y}$, respectively. The generalizations of (2.15a)–(2.15c) are then found to be

$$\Sigma\dot{X}=\{\varepsilon-q_1\}X-a\bar{Y}Z-X\{R_1|X|^2+P|Y|^2+P|Z|^2\}\ , \tag{2.16a}$$

$$\Sigma\dot{Y}=\{\varepsilon-q_2\}Y-a\bar{X}Z-Y\{R_1|Y|^2+P|X|^2+P|Z|^2\}\ , \tag{2.16b}$$

$$\Sigma\dot{Z}=\{\varepsilon-[2\bar{\lambda}_1\cos\Omega t]^2\}Z-aXY-Z\{R_1|Z|^2+P|X|^2+P|Y|^2\}\ , \tag{2.16c}$$

with $q_1=(\bar{\lambda}_1\cos\Omega t-\bar{\lambda}_2\cos[\Omega t+\gamma])^2$, $q_2=(\bar{\lambda}_1\cos\Omega t+\bar{\lambda}_2\cos[\Omega t+\gamma])^2$.

Here, for convenience, we have defined $\bar{\lambda}_1=(\pi^2/2)\lambda^{*1/2}\hat{\lambda}_1$, $\bar{\lambda}_2=(\sqrt{3}/2)\pi^2\lambda^{*1/2}\hat{\lambda}_2$. In general, closed form solutions of (2.16a)–(2.16c) are not available. Therefore, our aim in the following section will be to find the effect of the terms proportional to $\bar{\lambda}_1$ and $\bar{\lambda}_2$ on the bifurcation structure associated with hexagonal and roll cells.

III. THE SOLUTION OF THE AMPLITUDE EQUATIONS

In order to make analytical progress with the solution of (2.16a)–(2.16c), we now assume that $\Omega \gg 1$. With reference to the discussion given at the start of this section, we first let $\delta \to 0$ with Ω fixed and then consider the limit of large Ω; see Sec. IV for further discussion. If we confine our attention to $2\pi/\Omega$ periodic solutions, then for $\Omega \gg 1$ the amplitude equations can be solved using a multiple scale approach. We write

$$T = \Omega t$$

so that $\partial_t \to \partial_t + \Omega \partial_T$ and seek a solution of the form

$$(X, Y, Z) = (X_0, Y_0, Z_0) + \frac{1}{\Omega}(X_1, Y_1, Z_1) + \cdots , \tag{3.1}$$

where X_0, X_1, Y_0, etc. are functions of t and T. At order Ω we obtain

$$X_{0T} = Y_{0T} = Z_{0T} = 0$$

so that X_0, Y_0, and Z_0 are functions only of t. At order Ω^0 the equation to determine X_1 is found to be

$$-\Sigma X_{1T} = -\Sigma X_{0t} + \{\varepsilon - q_1\} X_0 - a\bar{Y}_0 Z_0 - X_0\{R_1|X_0|^2 + P|Y_0|^2 + P|X_0|^2\}$$

together with similar equations for Y_1 and Z_1. If these equations are to have a solution period in T, we require that

$$\Sigma X_{0T} = \{\varepsilon - \tfrac{1}{2}\bar{q}_1\} X_0 - a\bar{Y}_0 Z_0 - X_0\{R_1|X_0|^2 + P|Y_0|^2 + P|Z_0|^2\} , \tag{3.2a}$$

$$\Sigma Y_{0T} = \{\varepsilon - \tfrac{1}{2}\bar{q}_2\} Y_0 - a\bar{X}_0 Z_0 - Y_0\{R_1|Y_0|^2 + P|X_0|^2 + P|Z_0|^2\} , \tag{3.2b}$$

$$\Sigma Z_{0T} = \{\varepsilon - 2\bar{\lambda}_1^2\} Z_0 - aX_0 Y_0 - Z_0\{R_1|Z_0|^2 + P|X_0|^2 + P|Y_0|^2\} , \tag{3.2c}$$

with

$$\bar{q}_1 = [\bar{\lambda}_1^2 + \bar{\lambda}_2^2 - 2\cos\gamma\bar{\lambda}_1\bar{\lambda}_2], \bar{q}_2 = [\bar{\lambda}_1^2 + \bar{\lambda}_2^2 + 2\cos\gamma\bar{\lambda}_1\bar{\lambda}_2]$$

in the periodic case. For the case of steady shear we multiply $\bar{q}_1, \bar{q}_2$ by 2 and set $\gamma = 0$. The fact that only the mean values of q_1, q_2, etc. are required for $\Omega \gg 1$ allows this case to be discussed along with the steady flow case. The asymptotic solution given above for $\Omega \gg 1$ can be continued to arbitrary order and is suggested by, for example, setting $Y = Z = 0$ in (2.16) and letting $\Omega \to \infty$ in the exact solution of the resulting equation for X.

The above equations with $\partial_t = 0$ determine the equilibrium amplitude solutions of the problem with zero shear flow if $\bar{\lambda}_1 = \bar{\lambda}_2 = 0$, and their bifurcation structure for this case is therefore as described in [1,3]. In the presence of a shear flow we see that the bifurcation points for the pure modes with just one of $\bar{X}_0$, $\bar{Y}_0$, and $\bar{Z}_0$ nonzero are split apart. It is the splitting of the eigenvalues that causes the hexagonal mode to disappear in the presence of a sufficiently large shear flow. In order to see why this is the case, it is instructive to first recap the well known results for the case $\bar{\lambda}_1 = \bar{\lambda}_2 = 0$. Here the amplitudes X_0 and Y_0 are taken to be equal and, taking X_0, Y_0, Z_0 to be real, we find from [1] that the possible solutions are

(I) Conduction:

$$X_0 = Y_0 = Z_0 = 0 , \tag{3.3a}$$

(IIa,b) Rolls:

$$X_0 = Y_0 = 0, \quad Z_0 = \pm\left\{\frac{\varepsilon}{R_1}\right\}^{1/2} , \tag{3.3b}$$

(IIIa,b) Hexagons:

$$X_0 = Y_0 = Z_0, \quad Z_0 = (2T)^{-1}\{-a \mp \sqrt{a^2 + 4\varepsilon T}\} , \tag{3.3c}$$

(IVa,b) Hexagons:

$$X_0 = Y_0 = -Z_0, \quad Z_0 = (2T)^{-1}\{-a \mp \sqrt{a + 4\varepsilon T}\} , \tag{3.3d}$$

(V) Mixed:

$$Z_0 = -\frac{a}{Q}, \quad X_0 = Y_0 = \pm R^{1/2}\left[\varepsilon - \frac{R_1 a^2}{Q^2}\right]^{1/2} , \tag{3.3e}$$

where $Q = P - R_1, 4R = P + R_1$ and $T = P + 4R$.

The equilibrium forms for Z_0 given by (3.3a)–(3.3e) are shown in Fig. 1; the solutions shown correspond to the case $\sigma = 0.5$, $a = 1$. The other constants appearing in

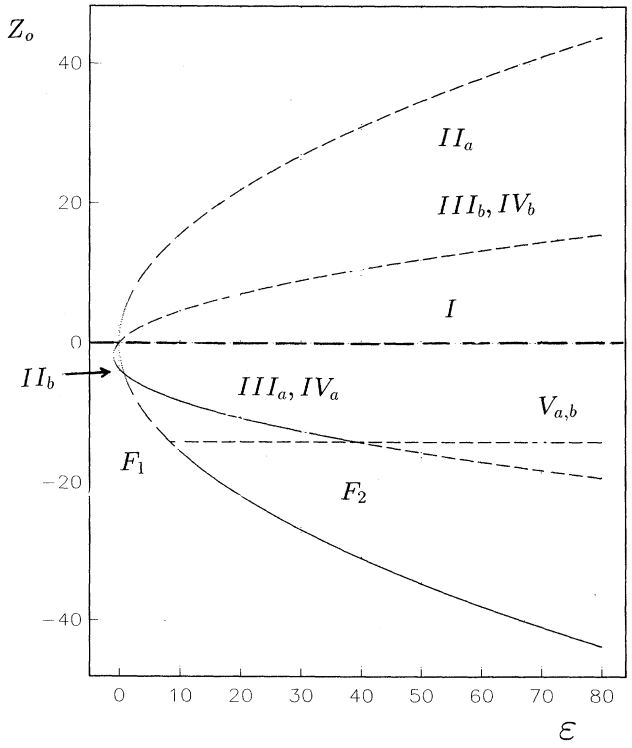

FIG. 1. The equilibrium solutions of (3.2) for $\bar{\lambda}_1^2 = \bar{\lambda}_2^2 = 0$. Unstable solutions are represented by the dashed curves.

(3.3) were obtained from [3]. The stability of the different solutions can be found by an examination of the linear growth rates of small perturbations to (3.3a)–(3.3e) in the manner discussed in the Appendix of [3] by use of (3.2a)–(3.2c). The unstable solutions are represented by the dashed curves in Fig. 1.

The zero amplitude solution loses stability at $\varepsilon=0$ so that a hexagonal pattern corresponding to IIIa or IVa will be generated when the Rayleigh number is slowly increased through zero. However, the hexagonal pattern loses stability at F_2 due to the effect of the mixed mode V even though this mode is unstable. The latter mode originates as a bifurcation from the roll mode at F_1. Beyond F_1 the roll mode IIb becomes stable. It follows that beyond F_2 the hexagonal cell pattern is replaced by a roll pattern. However, if the Rayleigh number is subsequently decreased, hysteresis occurs and the cellular pattern is not reestablished until F_1.

Now let us show how the above bifurcation picture is modified by the effect of a shear flow. The first point to note about the solutions of (3.2a)–(3.2c) in general is that the hexagonal solution $\bar{X}_0=\bar{Y}_0=\bar{Z}_0$ is no longer possible because, except in special circumstances, the three modes have different critical values of ε corresponding to linear instability. In the first instance we suppose $\bar{\lambda}_1=0$ so that the shear flow is parallel to the direction of the roll solutions IIa,b. The finite amplitude states are then found by solving

$$0=\left\{\varepsilon-\frac{\bar{\lambda}_2^2}{2}\right\}X_0-a\bar{Y}_0Z_0-X_0\{R_1|X_0|^2+P|Y_0|^2+P|Z_0|^2\}\ , \tag{3.4a}$$

$$0=\left\{\varepsilon-\frac{\bar{\lambda}_2^2}{2}\right\}Y_0-a\bar{X}_0Z_0-Y_0\{R_1|Y_0|^2+P|X_0|^2+P|Z_0|^2\}\ , \tag{3.4b}$$

$$0=\varepsilon Z_0-aX_0Y_0-Z\{R_1|Z_0|^2+P|X_0|^2+P|Y_0|^2\}\ . \tag{3.4c}$$

In this case we see that the X_0, Y_0 modes have the same linear critical value of ε; this enables us to seek finite amplitude states with $X_0=Y_0$. However, in order to correctly describe the stability properties of the finite amplitude states, we will relax the latter condition at a later stage.

The solutions IIa and IIb given by (3.3a) and (3.3b) survive unchanged because the effect of the shear flow is felt only by modes not aligned parallel to the shear. Equations (3.4a)–(3.4c) can then be solved with $X_0=Y_0\neq 0$ and $Z_0\neq 0$; Z_0 must then satisfy the cubic equation

$$a\left[\varepsilon-\frac{\bar{\lambda}_2^2}{2}\right]+Z_0\{\varepsilon(2P-4R)-a^2-P\lambda_2^2\}-3aPZ_0^2+Z_0^3[4R+P][4R-2P]=0\ . \tag{3.5}$$

If we set $\bar{\lambda}_2=0$, then we can factorize the above cubic equation to obtain the finite amplitude solutions III, IV, V of (3.3a)–(3.3e). Moreover, in the limit $\varepsilon\to\infty$ with $\bar{\lambda}_2$ held fixed, we again recover III, IV, V of (3.3a)–(3.3e). Figure 2 shows how the bifurcation picture for III, IV, V is initially modified for a relatively small value of $\bar{\lambda}_2=0.4$. The main point is that the modes IIIb and IVb no longer connect with IIIa and IVa, a fact that is more readily seen in Fig. 3, where the area near the origin is expanded. In fact IIIa and IVa now arise as bifurcations from the roll mode IIb. The unstable solutions are again represented by dashed curves. Point F_2 of Fig. 1 splits up into points F_2^+ and F_2^-, and the solution branch corresponding to IIIa and IVa is stable in the interval from F_3 to F_2^-. For small values of $\bar{\lambda}_2$ the solutions IIIa and IVa are close to those given by (3.3c) and (3.3d) so that the cell pattern is almost hexagonal; see Fig. 6 later. Since IIIa and IVa correspond to a hexagonal cell pattern when the shear is zero, we shall refer to them below as "modified hexagonal" solutions. We note from Fig. 2 that the roll cell IIb is stable in a small interval beyond $\varepsilon=0$ until the unstable branches of IIIa and IVa bifurcate from that solution branch at F_4 (see Fig. 3). Hence, if the background disturbance level is sufficiently small, it is possible for the initial cell pattern to be in the form of rolls even for an arbitrarily small shear flow. However, this roll pattern persists only over a small interval near $\varepsilon=0$ and is possibly not accessible experimentally.

In Fig. 3 we show how the bifurcation picture evolves when the shear flow is increased. We see that the turning point F_3 of Fig. 2 eventually merges into F_4, at which stage the modified hexagonal mode arises as a stable supercritical bifurcation from a stable roll. Similarly, F_2^- merges with F_1, at which stage the modified hexagonal

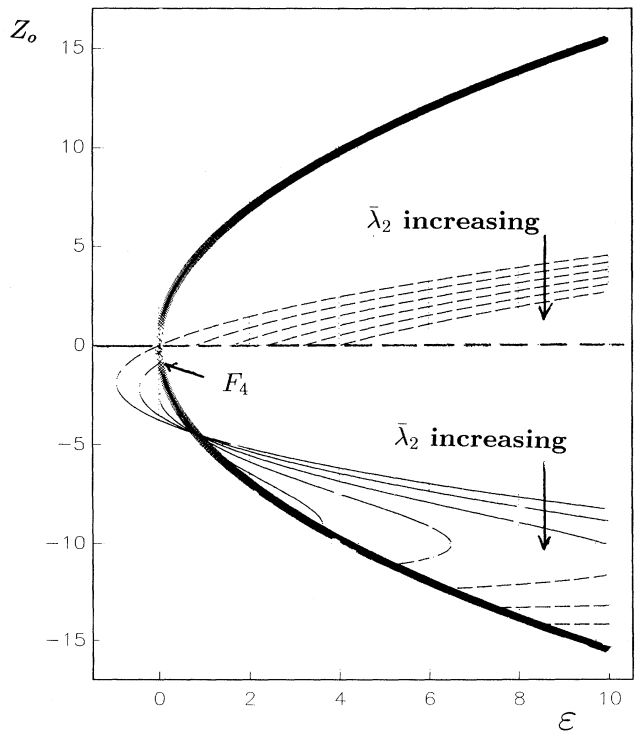

FIG. 2. The equilibrium solutions of (3.2) for $\bar{\lambda}_2^2$ relatively small. Unstable solutions are represented by the dashed curves.

mode merges smoothly into a stable roll and no hysteresis would be observed experimentally. At even higher values of the shear F_1 and F_4 merge and no stable remnant of IIIa and IVa of (3.3c) and (3.3d) remains. Thus IIb is now stable for all of the values of $\varepsilon > 0$ for which it exists. Therefore, at this stage we conclude that the shear flow has completely destroyed the possibility that convection of any pattern other than roll cells can occur. It is easy to show from (3.4a)–(3.4c) that $\bar{\lambda}_{2c}$, the critical value of $\bar{\lambda}_2$ where the points of secondary bifurcation from the roll mode merge, is given by

$$\bar{\lambda}_{2c}^2 = \frac{a^2}{2[P-R_1]} . \tag{3.6}$$

By definition, the corresponding critical value of $\bar{\lambda}_2$ is given by

$$\bar{\lambda}_{2c}^2 = \frac{3\pi^4 \lambda^* \hat{\lambda}_{2c}^2}{4} .$$

The critical Reynolds number for the flow is then given by

$$\sigma R_{ec} = \delta \hat{\lambda}_{2c} .$$

In Fig. 4 we show a plot of $\hat{\lambda}_{2c} a^{-1}$ as a function of the Prandtl number. The corresponding critical value of the Reynolds number is then found by calculating the appropriate value of a for the given fluid. In fact, since our method is valid also for the case of rigid boundaries, it seems sensible to give an estimate of the critical Reynolds number for that case. In order to do so, we use the values of the nonlinear coefficients given by Pampaloni *et al.* [13] for water at 25 °C. The constants P and R_1 were obtained from [4] and Pampaloni *et al.* found excellent agreement with their experimentally predicted values of these constants. The constant a is related to the constant $\mathcal{P}$ of Pampaloni *et al.*, who quote a theoretical value of 2.06 for it. The experimental measurements of [13] showed that $\mathcal{P}$ is in the range (0–2.63), and the lack of agreement between theory and experiment is due to the uncertainty about the fluid properties needed to define $\mathcal{P}$ and the experimental uncertainties associated with the onset and ending of hexagonal convection. In order to make a prediction for the rigid case, we take $\mathcal{P}$ to be 2.06 and with the value of λ^* taken from [10] we find that the critical value for the steady flow Reynolds number above which convection cannot take place is 2.1. The latter result is consistent with [6], where it was stated that hexagonal convection was not observed at Reynolds numbers greater than 10 for air.

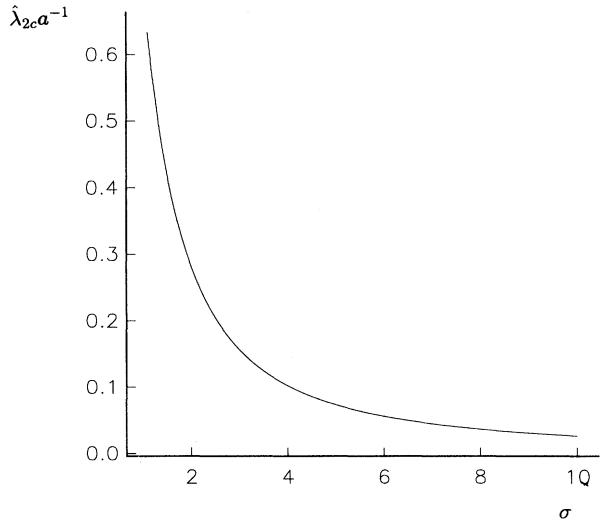

FIG. 4. The quantity $\hat{\lambda}_{2c} a^{-1}$ as a function of the Prandtl number.

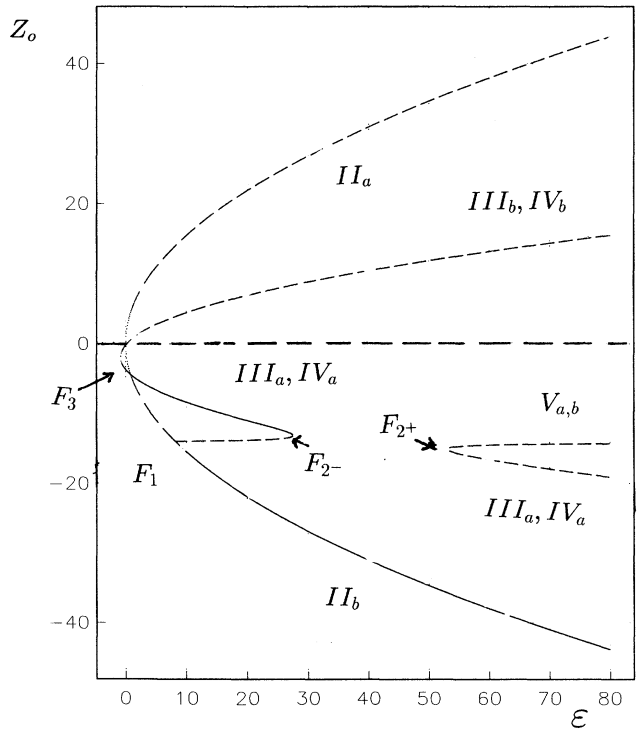

FIG. 3. The equilibrium solutions of (3.2) for the case $\sigma = 0.5$, $a = 1$, $\bar{\lambda}_1 = 0$, $\bar{\lambda}_2^2 = 0$, 1.6, 3.2, 4.8, 6.4, 8, ... Unstable solutions are represented by the dashed curves. The roll mode is represented by the thick curve and, for a fixed value of the shear, is unstable for positive amplitudes and stable for negative amplitudes apart from the interval between the points where secondary bifurcation takes place. Note that for large enough shear flows, the latter interval is not present and the roll mode is stable whenever it has a negative finite amplitude.

In Fig. 5 the loci of the points F_2^- and F_3 in the $(\varepsilon, \bar{\lambda}_2^2)$ plane are denoted by the curves C_4 and C_1, respectively. Curves C_2 and C_3 represent the loci of the points of secondary bifurcation from the lower branch of the roll mode. Point M_2 where C_1 and C_2 meet corresponds to the position where F_3 merges with F_4. Similarly, M_1 corresponds to the point where F_2^- and F_1 merge. It is perhaps useful at this stage to discuss the implications of Fig. 5 for any experimental investigation of the effect of a shear flow on convection patterns. In the first instance we suppose that the shear is fixed at a value corresponding to a point to the left of a vertical line through M_1 in Fig. 5. In this case, no convection occurs until C_4 is

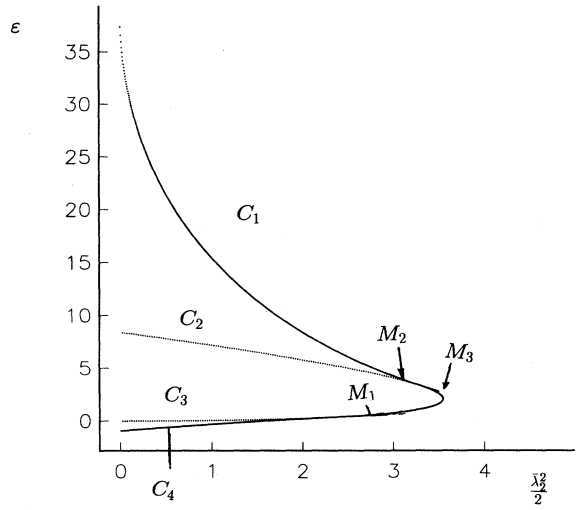

FIG. 5. The loci of points F_2^- and F_3 in the ε-$\bar{\lambda}_2^2$ plane are denoted by curves C_1 and C_2, respectively. Curves C_2 and C_3 represent the loci of the points of secondary bifurcation from the lower branch of the roll mode. The solutions shown correspond to the case $\sigma=0.5$, $a=1$.

crossed. At this stage, a discontinuous jump to a modified hexagonal mode will occur if the experimental noise is sufficiently large. The size of the noise needed to trigger the convection decreases when $\bar{\lambda}_2$ increases. Between the horizontal axis and C_3, a small amplitude stable roll is possible although for small values of the shear it would probably not be excited, since at that stage a larger amplitude modified hexagonal cell would already be established.

When C_2 is crossed, a stable roll is again possible, while beyond C_1 the modified hexagonal cell is unstable, so that a roll cell aligned with the shear is the only stable state. The switch from the modified hexagonal cell to the roll cell leads to a discontinuous jump in the amplitude of convection, and hysteresis occurs when ε is subsequently decreased. Thus, at this stage the introduction of shear flow has had only a slight effect on the zero-shear bifurcation picture. More precisely, the range over which the modified hexagonal cell exists has been decreased and the possibility of small amplitude roll convection when the Rayleigh number crosses the linear critical value now exists. The likelihood of the latter event taking place increases as the shear increases, since C_4 approaches C_3 in that case.

Now suppose that the shear is fixed at a value corresponding to a point between vertical lines through M_1 and M_2. The modified hexagonal mode now bifurcates supercritically from the weak roll cell. Furthermore, the onset of convection leads in this case to the formation of a weak roll which subsequently suffers a secondary bifurcation to the modified hexagonal cell. At higher values of ε the picture is unchanged, and hysteresis will occur.

The next regime occurs when the shear is between the values corresponding to M_2 and M_3 in Fig. 5. Now the modified hexagonal cell loses stability to a roll cell, and hysteresis no longer occurs. Thus, when the Rayleigh number is increased through its linear critical value, convection first appears as a supercritical bifurcation to a roll cell. The roll cell then suffers a secondary bifurcation to a modified hexagonal cell, which, itself, loses stability back to the roll cell. Thus, in this regime the amplitude of convection changes continuously when the Rayleigh number increases or decreases. Finally, if the shear is further increased, the roll cell is stable at all Rayleigh numbers and the modified hexagonal cell is never present.

Thus we have seen that between C_1 and C_4, convection with a planform other than streamwise rolls can occur. In fact, the cell pattern in this interval is shown in Fig. 6(a)–6(d) for different values of $\bar{\lambda}_2^2$ at a fixed value of $\varepsilon=20$. The contours correspond to the disturbance temperature at $z=\frac{1}{2}$. We see that the shear flow deforms the hexagonal shaped cells of the zero shear case. However, even at a value of the shear flow just before F_1 and F_4 merge [Fig. 6(d)], a roll pattern has not been established. Thus, as in the zero shear case, there is a discontinuous change in the cell pattern when the roll cell becomes the only stable state. Note also that for even higher values of $\bar{\lambda}_2^2$ the only possible stable finite amplitude cell is the roll cell. Figures 6(a)–6(d) can be usefully compared to Figs. 5(a) and 5(b) of [14], in which the evolution of rolls from hexagons is shown from experiment for the nonzero shear case.

As another special case that enables us to make analytical progress, we now suppose that the shear flow is in a direction at right angles to the roll solution $X_0=Y_0=0$, $Z_0\neq 0$. Thus we now set $\bar{\lambda}_2=0$ and we can again seek solutions of (3.2) with $X_0=Y_0$ and X_0, Y_0, Z_0 all real. The appropriate form of (3.2) is then found to be given by

$$0=\left\{\varepsilon-\frac{\bar{\lambda}_1^2}{2}\right\}Y_0-aY_0Z_0-Y_0\{4RY_0^2+PZ_0^2\}\ , \tag{3.7a}$$

$$0=\{\varepsilon-2\lambda_1^2\}Z_0-aY_0^2-Z_0\{R_1Z_0^2+2PY_0^2\}\ . \tag{3.7b}$$

Thus we see that the Y mode now becomes linearly unstable before the Z mode. The roll modes IIa and b again exist (but with a shift of origin) and, by eliminating Y_0, we can derive a cubic equation for Z_0. In fact, the equation is obtained directly from (3.5) by a shift of origin in ε.

The finite amplitude solutions for the case $\sigma=0.5$, $a=1$, and a range of values of $\bar{\lambda}_1$ are shown in Fig. 7. The solution branches IIIb and IVb now bifurcate from IIa supercritically while IIIa and IVa initially bifurcate subcritically from the zero state. For small values of $\bar{\lambda}_1$, these branches are stable for a finite range of values of ε between the turning point labeled F_3 and the point labeled F_7 on the curve shown for the smallest value of $\bar{\lambda}_1$. It is of interest to note that at point F_7, the solutions IIIa and IVa become unstable to a perturbation in X_0-Y_0 so that there exists a finite amplitude solution with $X_0\neq Y_0$ bifurcating from this point. We do not calculate that solution here, since it is almost certainly physically irrelevant for the reasons to be discussed below. We note that as $\bar{\lambda}_1$ increases point F_3 moves toward and finally hits the ε axis and IIIa and IVa arise from a supercritical bifurcation and are therefore stable until F_7. In fact, the

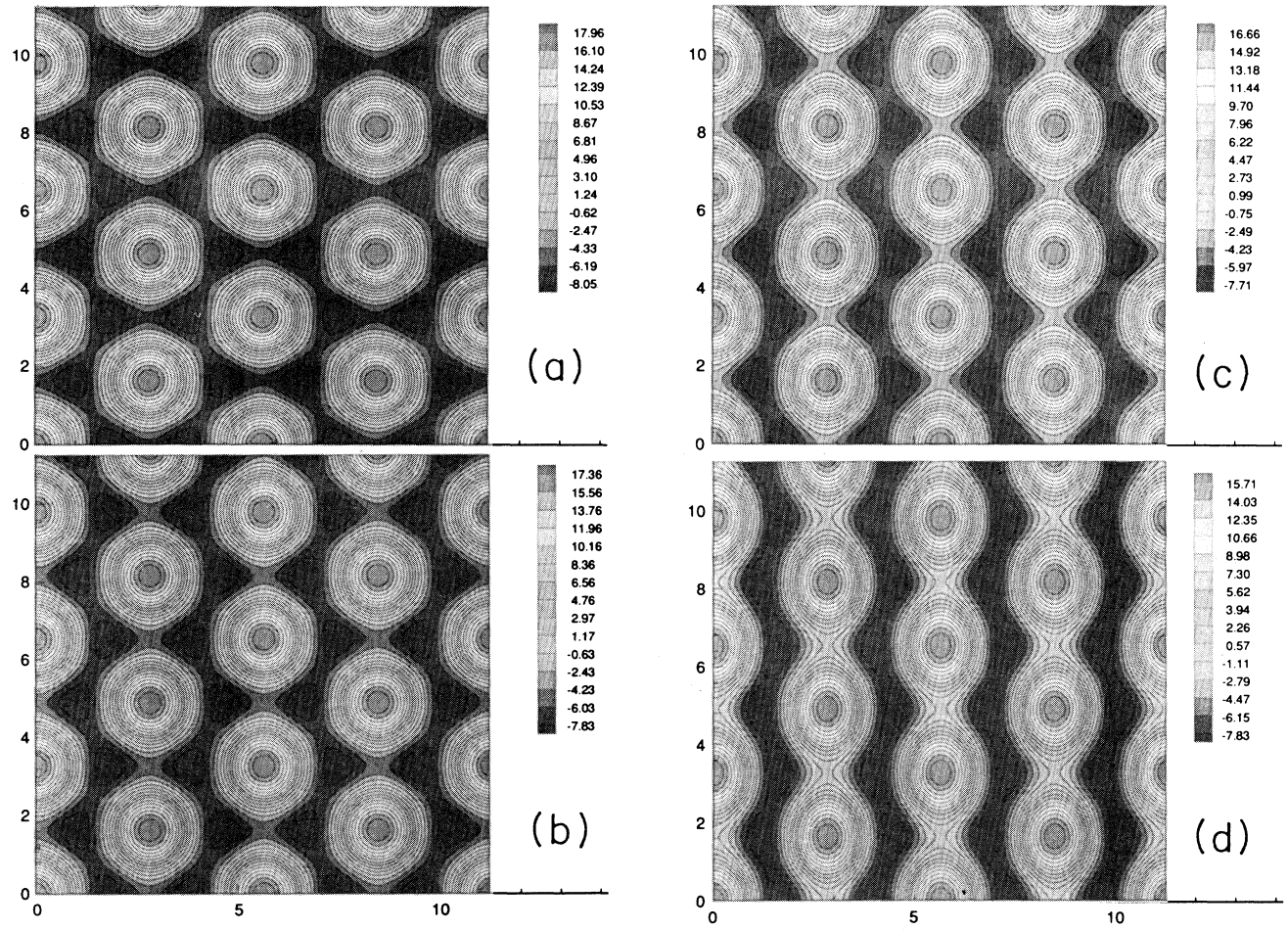

FIG. 6. Contours of constant disturbance temperature for the case $\sigma=0.5$, $a=0.1$, $\varepsilon=5$, $\bar{\lambda}_2^2=0$, 1.6, 3.2, 4.8.

band of stable solutions terminating at F_7 eventually disappears when F_7 hits the ε axis. The roll mode IIb is seen to be stable beyond the value of ε at which Va and Vb bifurcate as unstable solutions of the amplitude equations.

If we restrict our attention to the situation with $X_0=Y_0$, then the results shown in Fig. 7 indicate that the onset of convection will be in the form of almost hexagonal shaped cells until F_7 hits the ε axis. For values of $\bar{\lambda}_1$ greater than the critical value at which this occurs, the only possible stable finite amplitude state is that corresponding to IIb after the secondary bifurcation of Va and Vb. It follows that there is then a small band of values of ε beyond $2\varepsilon=\bar{\lambda}_1^2$ where no stable state exists. However, there is the possibility of a finite amplitude state with $X_0\neq Y_0$ but, since our analysis has not allowed for a roll cell parallel to the x axis, our results are probably only physically relevant until F_3 moves to the right of the Z_0 axis in Fig. 7. We believe this to be the case, since, from our discussion above for the case when the shear flow was parallel to the z axis, we know that such a roll state bifurcates supercritically from $\varepsilon=0$. However, these remarks must remain speculative until we extend our analysis to

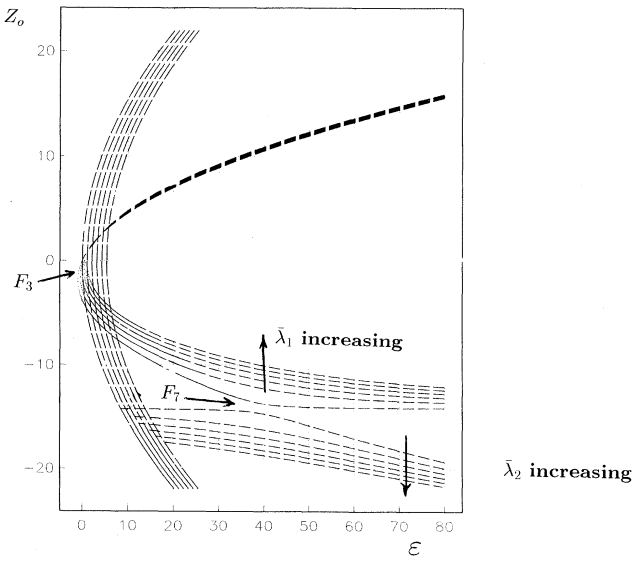

FIG. 7. The equilibrium solutions of (3.2) for the case $\sigma=0.5$, $a=9$, $\bar{\lambda}_2=0$, $(3\bar{\lambda}_1^2/2)=0.05$, 0.85, 1.65, 2.45, 3.25, 4.05. Unstable solutions are represented by the dashed curves.

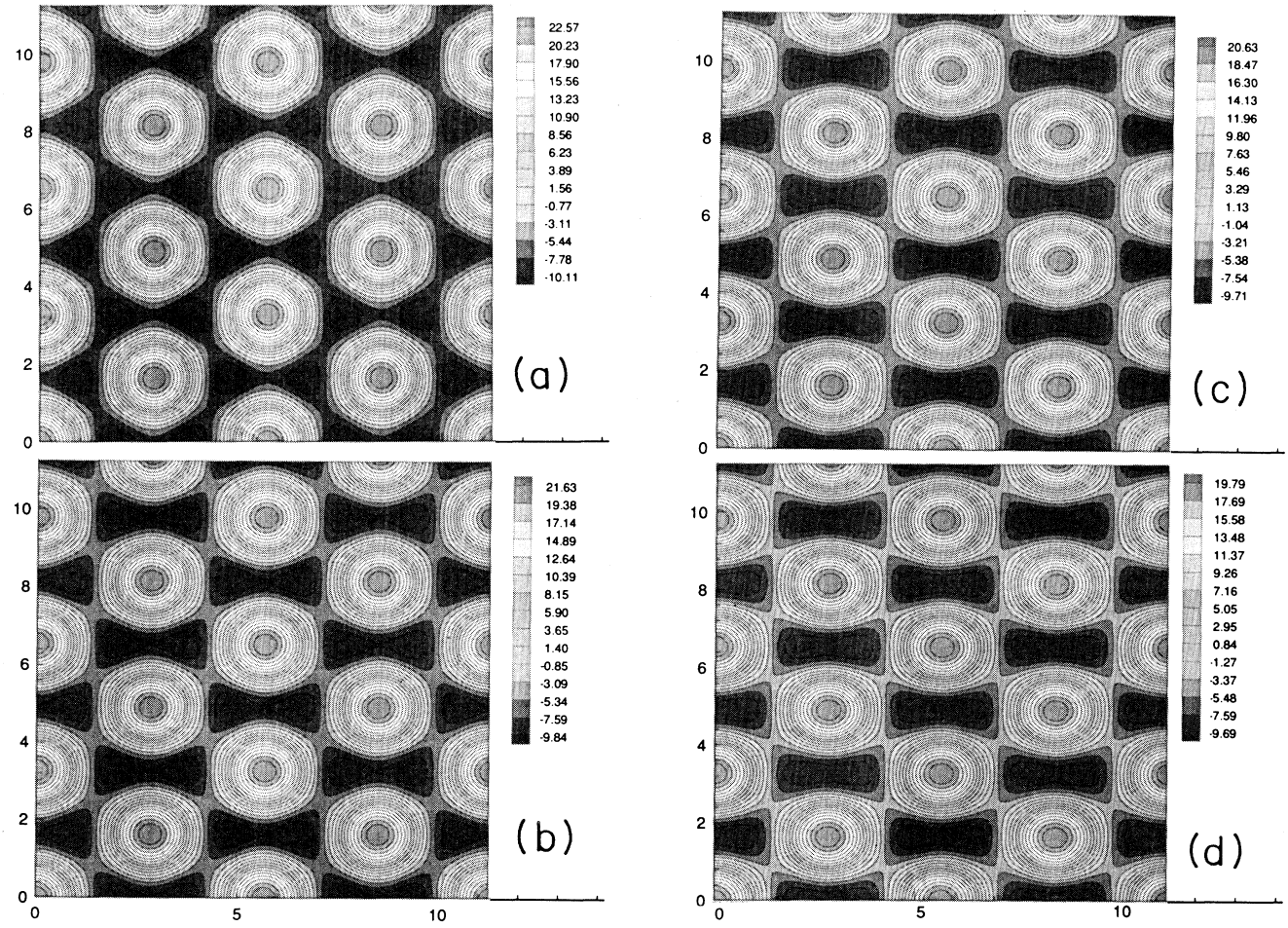

FIG. 8. Contours of constant disturbance temperature for the case $\sigma=0.5$, $a=1$, $\varepsilon=10$, $(2/3)\bar{\lambda}_1^2=0$, 1.6, 3.2, 4.8.

account for the interaction of more than three modes. If we assume that the roll mode parallel to the x axis will destabilize IIIa and IVa, then the critical value of $\bar{\lambda}_1$ at which F_3 crosses the Z_0 axis gives the size of the shear flow needed to cause the onset of convection to always be in the form of streamwise rolls. A calculation shows that this will happen when $\bar{\lambda}_1^2$ is approximately $9a^2$ with $\sigma=0.5$.

In Figs. 8(a)–8(d) we show contours of constant disturbance temperature at $z=\frac{1}{2}$ at different values of $\bar{\lambda}_1^2$ at a fixed value of $\varepsilon=10$. We see that the main effect of the shear flow is to generate increasingly strong cells in between the original hexagonal shaped cells. However, we note that if ε is increased slightly above zero a stable roll cell aligned with the basic shear flow is also possible; that solution is not described by our three mode analysis.

IV. FURTHER COMMENTS AND CONCLUSIONS

We have given a description of the process by which a shear flow destroys the preference of a fluid to support hexagonal cells at the onset of convection in a non-Boussinesq fluid. The amplitude equations we derived describe the effect of both constant and slowly varying unsteady nonplanar shear flows on the solutions of the amplitude equations of [1,3]. We have restricted our attention to a certain high frequency limit of the amplitude equations; this enables us to reduce (2.16) to an equivalent steady flow system (3.2). Note, however, that the high frequency limit we took was subsequent to the assumption that the convection and mean flow evolve on a long time scale so that, strictly speaking, our results correspond to a range of low frequencies. If the scaled frequency Ω is not large, then it appears that a numerical treatment of (2.16) is appropriate; we do not address that problem here. The analysis of [9] concerned only steady shear flows and was restricted to rolls aligned with the flow. The stability analysis given in [9] is incomplete, since it does not allow for perturbations with, in our notation, $X\neq Y$. Figure 2 of [9] is a sketch of the possible stable solutions found in Yoshizaki's qualitative analysis. There are some similarities with our Fig. 5 but the stability properties shown are in error for the reason given above.

The two cases we considered in detail correspond to the situation where the shear flow is at right angles or

parallel to the roll mode (of amplitude Z) in our three (complex) mode analysis. When the flow is aligned with the rolls, we find that, as indicated in Fig. 7, the shear flow causes the hexagonal cells to deform and become connected. This connection between the cells is caused by the fact that as the shear flow increases, the mode which, in the zero shear case, exhibits hexagonal cells has the ratio of the Z mode amplitude to the X, Y modes increasing. However, before the deformation of the hexagonal cells into rolls is complete, the mode loses stability to the "pure" Z roll mode. Some experimental results of the effect of a shear flow on convection cell patterns have been given by Graham [14]. Kelly [5] gives a summary of Graham's results and related work by Avsec and Luntz [15]. In Fig. 18 of [5], a sketch of the experimental results corresponding to Fig. 7 of this paper is given. The initial evolution shown in Figs. 18(a)–18(c) of [5] is consistent with our Figs. 6(a)–6(d). However, Figs. 18(d) and 18(e) of [5] suggest that the next step in the evolution process is the re-emergence of a hexagonal cell pattern rotated through 30 degrees from the original one. Our calculations do not allow for such a possibility, but it is interesting to note that at this stage we have the situation appropriate to our second special case with the flow in the x direction. The evolution shown in Figs. 8(a)–8(d) is then seen to be consistent with that shown in Fig. 18(f) of [5]. Thus it appears that there is some qualitative agreement between our theory and experimental observations. A more detailed comparison requires us to extend our analysis to allow for more possible interactions. In the meantime, it would be interesting to see if experiments could reproduce the theoretical trends associated with, for example, Fig. 5. Kimura *et al.* [16] investigated experimentally the effect of shear on thermal convection by use of an annular convection cell in which the flow as generated by moving the upper surface azimuthally. They observed an intermediate form of convection existing between cellular convection and longitudinal rolls that might correspond to our hexagonal cell pattern. However, Kimura *et al.* used a cell with an aspect ratio of only five, and the finite thermal conductivity at the upper surface initially caused rectangular cells to be observed rather than hexagons. They found a critical value of the shear, above which longitudinal rolls occur, that increases with Rayleigh number, but we cannot compare our results with their observations, since their data starts only at twice the critical Rayleigh number, which is outside the range of validity of our theory.

ACKNOWLEDGMENTS

This research was supported by The National Science Foundation under Grant No. NSF CTS-9123553 and by the Science and Engineering Research Council, U.K.

[1] L. A. Segel and J. Stuart, J. Fluid Mech. **13**, 289 (1962).
[2] E. Palm, T. Ellingsen, and V. Gjevik, J. Fluid Mech. **30**, 651 (1967).
[3] L. A. Segel, J. Fluid Mech. **21**, 359 (1965).
[4] F. H. Busse, J. Fluid Mech. **28**, 223 (1967).
[5] R. E. Kelly, Adv. Appl. Mech. **31**, 35 (1994).
[6] S. Ostrach and Y. Kamotani, J. Heat Transfer **97**, 220 (1975).
[7] A. P. Ingersoll, Phys. Fluids **9**, 682 (1966).
[8] H. W. Müller, M. Lücke, and M. Kamps, Europhys. Lett. **10**, 451 (1989).
[9] M. Yoshizaki, J. Meteor Soc. Jpn. **57**, 548 (1979).
[10] R. E. Kelly and H. C. Hu, J. Fluid Mech. **249**, 373 (1993).
[11] R. E. Kelly and H. C. Hu, in *Heat Transfer 1994,* edited by G. F. Hewitt (Hemisphere, New York, 1994), Vol. 7, p. 79.
[12] R. C. DiPrima and J. T. Stuart, J. Fluid Mech. **67**, 85 (1975).
[13] E. Pampaloni, C. Perez-Garcia, L. Albavetti, and S. Ciliberto, J. Fluid Mech. **234**, 393 (1992).
[14] A. Graham, Philos. Trans. R. Soc. London Ser. A **232**, 285 (1933).
[15] D. Avsec and M. Luntz, Meteorologie **3**, 180 (1937).
[16] R. Kimura, H. Tsu, and A. Yagihashi, J. Meteor. Soc. Jpn. **49**, 249 (1971).

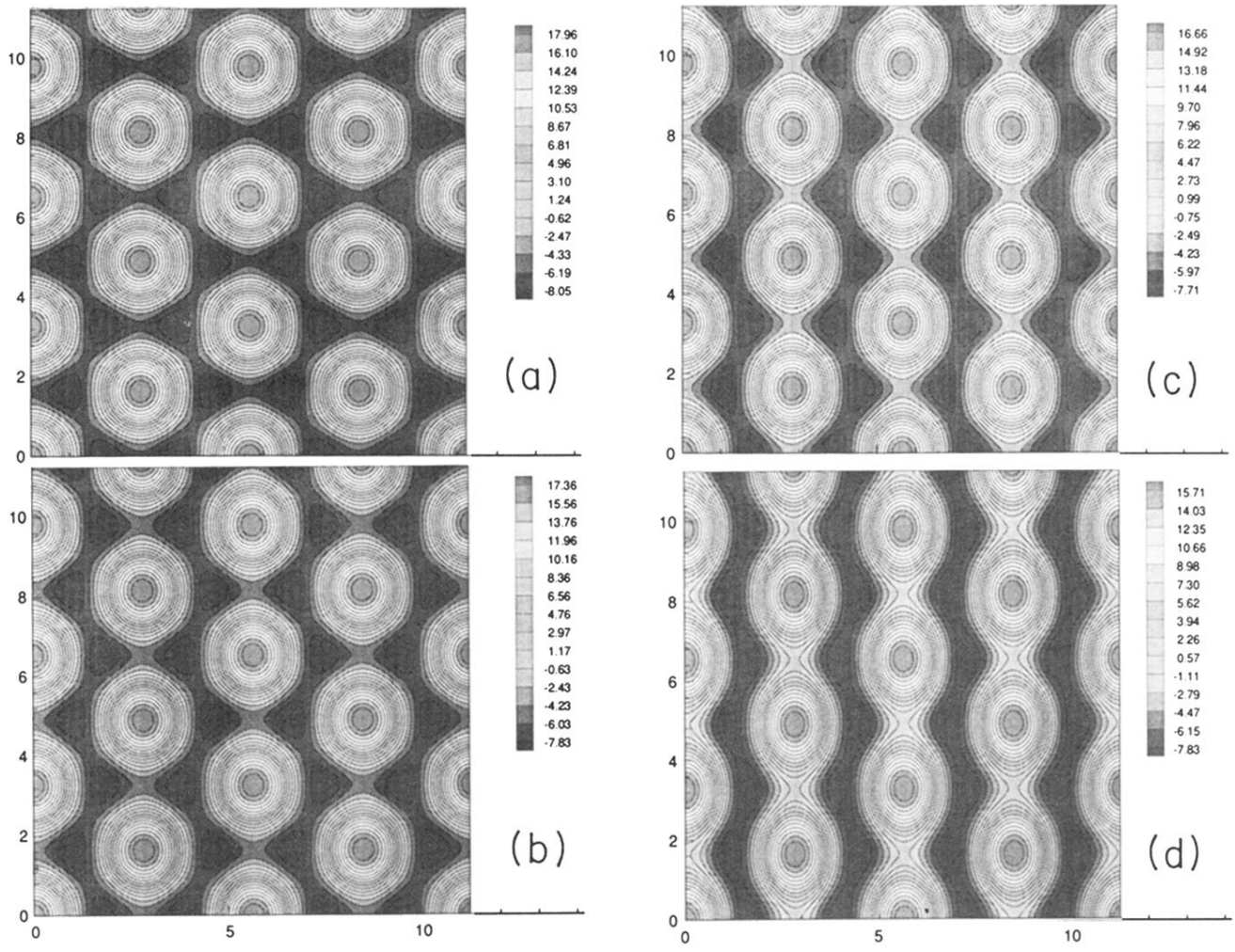

FIG. 6. Contours of constant disturbance temperature for the case $\sigma = 0.5$, $a = 0.1$, $\varepsilon = 5$, $\bar{\lambda}_2^2 = 0$, 1.6, 3.2, 4.8.

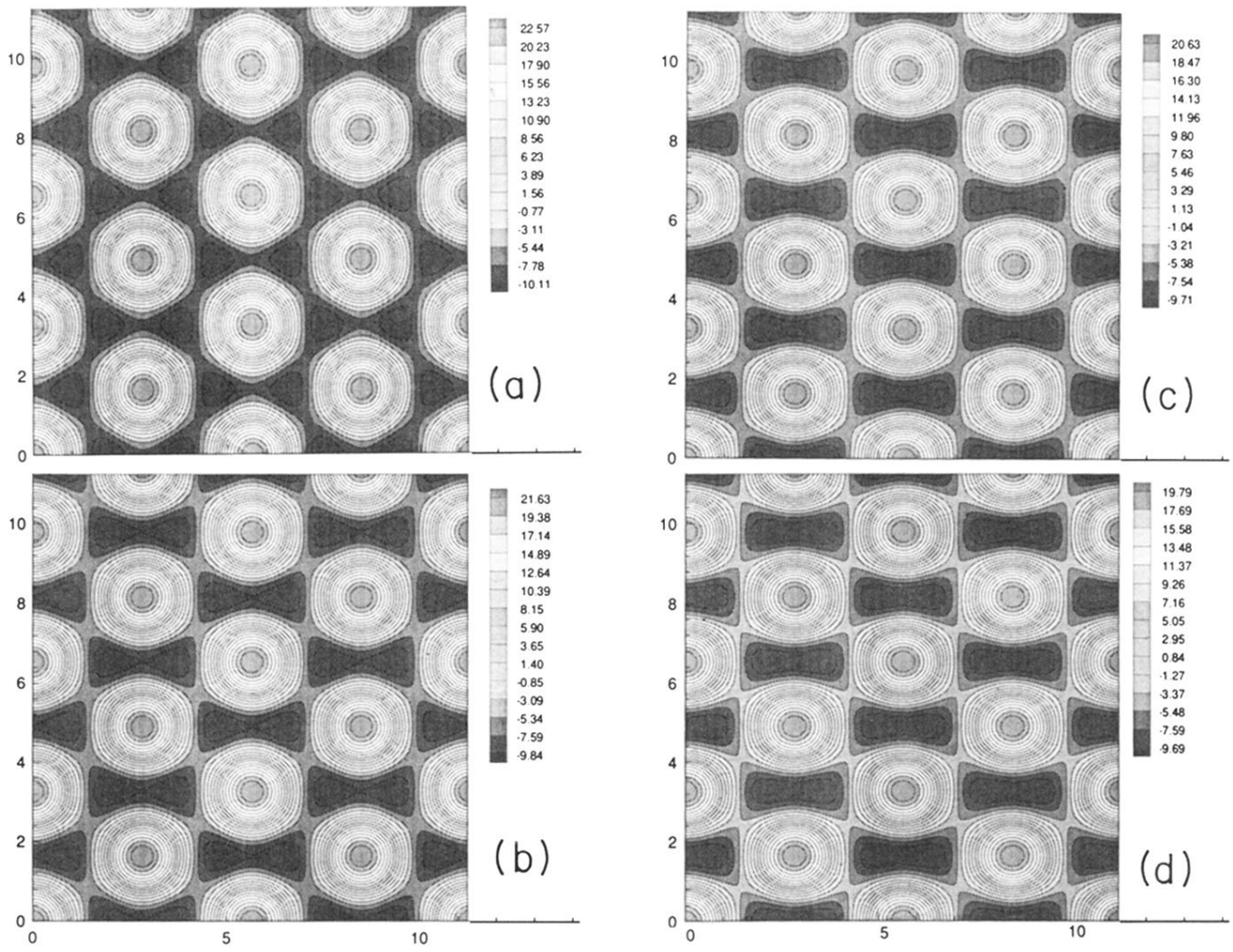

FIG. 8. Contours of constant disturbance temperature for the case $\sigma = 0.5$, $a = 1$, $\varepsilon = 10$, $(2/3)\bar{\lambda}_1^{-2} = 0$, 1.6, 3.2, 4.8.